

Deflection calculation method on GFRP-concrete-steel composite beam

Zhaojie Tong^a, Xiaodong Song^b and Qiao Huang^{*}

Department of Bridge Engineering, School of Transportation, Southeast University, Nanjing, China

(Received October 17, 2017, Revised December 20, 2017, Accepted December 21, 2017)

Abstract. A calculation method was presented to calculate the deflection of GFRP-concrete-steel beams with full or partial shear connections. First, the sectional analysis method was improved by considering concrete nonlinearity and shear connection stiffness variation along the beam direction. Then the equivalent slip strain was used to take into consideration of variable cross-sections. Experiments and nonlinear finite element analysis were performed to validate the calculation method. The experimental results showed the deflection of composite beams could be accurately predicted by using the theoretical model or the finite element simulation. Furthermore, more finite element models were established to verify the accuracy of the theoretical model, which included different GFRP plates and different numbers of shear connectors. The theoretical results agreed well with the numerical results. In addition, parametric studies using theoretical method were also performed to find out the effect of parameters on the deflection. Based on the parametric studies, a simplified calculation formula of GFRP-concrete-steel composite beam was exhibited. In general, the calculation method could provide a more accurate theoretical result without complex finite element simulation, and serve for the further study of continuous GFRP-concrete-steel composite beams.

Keywords: GFRP-concrete-steel; composite beam; deflection; finite element; slip; variable cross-sections

1. Introduction

Recently, various kinds of GFRP-concrete decks (Honickman *et al.* 2009, Cheng 2011, Nelson and Fam 2014) have been designed to increase the durability of bridge deck and some of these decks (Alagusundaramoorthy *et al.* 2006, Berg *et al.* 2006) have been applied in the bridge engineering. The GFRP-concrete decks include plate integrated with T-shape ribs (Nelson and Fam 2012), plate with tubular ribs (Dieter *et al.* 2002), corrugated FRP-concrete deck (He *et al.* 2012), dual cavity system (Cho *et al.* 2013), etc. A lot of research has been conducted to study the static mechanical performance of simply supported one-way decks, simply supported two-way decks and continuous decks. However, there were few studies on the composite action between steel beams and GFRP-concrete decks. The composite beam with T-shaped GFRP-concrete decks is shown in Fig. 1. The GFRP-concrete-steel composite beam consists of GFRP-concrete deck and steel beam. The cross sections of the composite beam are not uniform because of the effect of T-shaped ribs. The stress on the top surface of concrete in the T-shaped rib sections is higher than that of the cross-sections without T-shaped rib. Moreover, the load in the beam direction is shared by three kinds of materials (steel, GFRP and concrete). Therefore, the deflection calculation method of GFRP-concrete-steel composite beam is different from that

of steel-concrete composite beam. The variable cross-sections and the load shared by GFRP plate should be considered. The study on the calculation method is beneficial for application of GFRP-concrete decks in bridge engineering.

According to the proportion of GFRP plate in the GFRP-concrete deck, the static mechanical performance of GFRP-concrete-steel composite beam was similar to that of GFRP-steel composite beam or steel-concrete composite beam. For the calculation method of steel-concrete composite beam, a large number of studies have been conducted to provide more accurate results. Slip (Nie and Cai 2003, Nie *et al.* 2005, Wang 1998), shear lag (Goncalves and Camotim 2010, Huang *et al.* 2016, Zhou *et al.* 2015), shear deformation (Ranzi and Zona 2007) were considered in the theoretical model. Moreover, with the development of finite element method (FEM), the deflection can also be calculated by using numerical models (Aref *et al.* 2007, Khorramian *et al.* 2017, Samaaneh *et al.* 2016). For the GFRP-steel composite beam, the studies focused primarily on the calculation method of shear lag (Zou *et al.* 2011, Moses *et al.* 2006, Tenchev 1996). In general, the deflection could be predicted by using theoretical or numerical models. Complex finite element model could provide more accurate results. However, FEM is a time consuming process, especially for the nonlinear analysis. The theoretical method is rough, especially in the nonlinear analysis, but it is convenient and suitable for engineering design.

In present, there were few studies on the deflection calculation method of GFRP-concrete-steel composite beams. The theoretical model of steel-concrete/GFRP-steel composite beam could not exhibit the characteristic of GFRP-concrete-steel composite beam. Moreover, the

*Corresponding author, Professor,

E-mail: qhuanghit@126.com

^a Ph.D. Candidate, E-mail: tongzhaojie@seu.edu.cn

^b Ph.D., E-mail: xdsong@seu.edu.cn

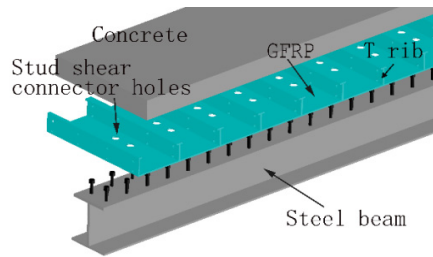


Fig. 1 GFRP-concrete-steel composite beam

existing theoretical model of steel-concrete/GFRP-steel composite beam was usually based on the assumption of linear material and constant shear connector stiffness. The nonlinear results could only be obtained by using amended modulus and shear connector stiffness in a certain section. In fact, the modulus of concrete and the shear connector stiffness varied from one section to another along the beam direction. The deflection result was not accurate without consideration of the variation in the beam direction.

This paper presents a theoretical calculation method of GFRP-concrete-steel composite beam. This model could consider concrete nonlinearity, shear connector stiffness variation from one section to another, and variable cross-sections caused by GFRP plate. First, the sectional analysis method (Zheng *et al.* 2016, Wang *et al.* 2013) was improved to consider the slip between GFRP-concrete deck and steel beam. The calculation method of steel-concrete composite beam based on the improved sectional analysis method was exhibited, which could consider slip and concrete nonlinearity. Then the equivalent slip was used to consider the variable cross-sections, and the calculation method of steel-concrete composite beam was extended for calculation of GFRP-concrete-steel composite beam. A computer program was written to implement the deflection calculation method. The deflection could be quickly obtained by using the computer program, and the computer program is beneficial for bridge design. The deflection calculation method was validated by finite element simulation and experiment. Moreover, parametric analysis was conducted by using the theoretical model. Based on the results of parametric analysis, a simplified deformation calculation formula of GFRP-concrete-steel composite beam was presented.

2. Deflection calculation model

The deflection of steel-concrete composite beam with consideration of slip can be calculated by using Chinese standard JTG/T D64-2015. However, the calculation method is based on the assumption of constant shear connector stiffness. For composite beams with full shear connectors, as the shear force shared by each shear connector is low, the deflection could be calculated with constant shear connector stiffness. For the composite beams with partial shear connector, as the shear force shared by each shear connector is high, there is a significant shear connector stiffness variation along the beam direction, and the deflection could not be obtained by using constant shear

connector stiffness. Moreover, the cross-sections of GFRP-concrete-steel composite beam are variable. The deflection calculation method should consider both slip and variable cross-sections. Therefore, the calculation method of GFRP-concrete-steel composite beam is more complex than that of steel-concrete composite beam. In this section, the calculation method of steel-concrete composite beam is firstly exhibited, which considers concrete nonlinearity and shear connector stiffness variation. Then the calculation method of GFRP-concrete-steel composite beam is exhibited, which considers concrete nonlinearity, shear connector stiffness variation and variable cross-sections. This calculation method could predict the deflection before the composite beam achieves the elastic bending moment capacity.

The Chinese standard JTG/T D64-2015 suggests the neutral axis of composite beams locates in the steel beam. The theoretical model is based on the situation that the neutral axis location is within the steel beam. When the neutral axis location is within the concrete, the theoretical derivation is similar. Moreover, as the stud shear connector is the most common type of shear connectors, the constitutive relationship of stud shear connector is used in the deflection calculation model.

2.1 Deflection calculation model of steel-concrete composite beam

The transformed section method is a common calculation method of steel-concrete composite beams. However, the transformed section method is based on constant modulus, and the nonlinear deflection could not be accurately simulated. The full load-deflection response could be predicted by using sectional analysis method, as the nonlinear concrete constitutive relationship is used. But the slip is ignored in the sectional analysis method. Consequently, the application of the sectional analysis method is seldom used in the deflection calculation of composite beams considering slip. In order to consider slip and concrete nonlinearity, the sectional analysis method is improved in this study.

2.1.1 Constitutive relationships

In order to predict the deflection before the composite beam achieves the elastic bending moment capacity, the constitutive relationships are as follows:

The relationship of stress and strain of concrete can be written as

$$\begin{cases} \sigma_c = f_c \left[2 \frac{\varepsilon_c}{\varepsilon_0} - \left(\frac{\varepsilon_c}{\varepsilon_0} \right)^2 \right] & (0 \leq \varepsilon \leq \varepsilon_0) \\ \sigma_c = f_c & (\varepsilon > \varepsilon_0) \end{cases} \quad (1)$$

where $\varepsilon_0 = 0.002$; f_c is the concrete strength; ε_c is the concrete strain; σ_c is the concrete stress.

The load-slip relationship of stud shear connector can be written as

$$V / V_u = (1 - e^{-a\Delta_s})^b \quad (2)$$

where V_u is the shear capacity of stud shear connector; V is the shear force shared by shear connector; Δ_s is the slip; a

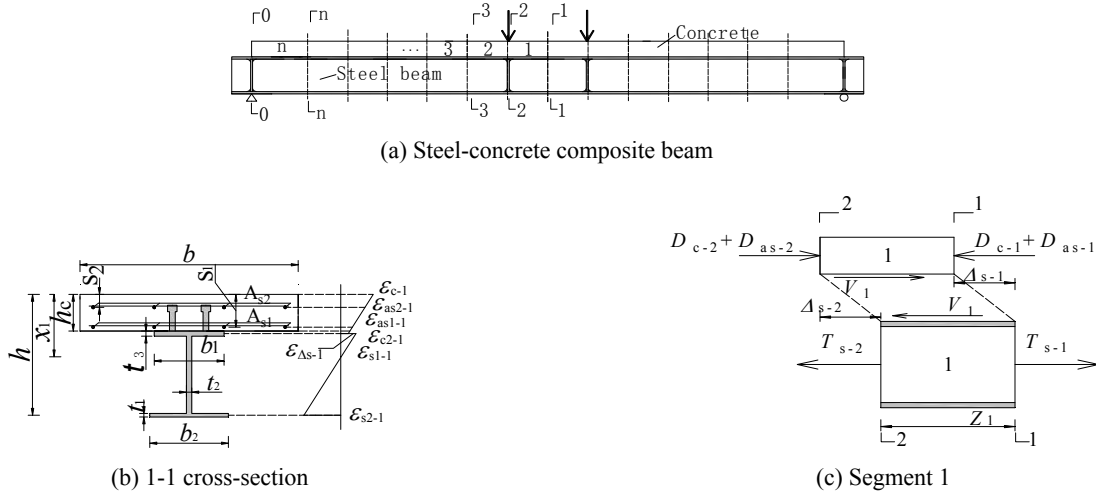


Fig. 2 Deflection calculation model of steel-concrete composite beam

and b can be obtained with experiments.

For the stud shear connector with stud failure, the shear capacity (Hanswille *et al.* 2007a, b) of stud shear connector can be written as

$$V_u = A_s f_u \quad (3)$$

where A_s is the area of stud shear connector; f_u is the tensile strength of stud shear connector.

For the stud shear connector with concrete failure, the shear capacity of stud shear connector in JTG D64-01-2015 can be written as

$$V_u = 0.43 A_s \sqrt{E_c f_c} \quad (4)$$

where E_c is the modulus of concrete.

The relationship of stress and strain of steel beam or steel reinforcement can be written as

$$\sigma_s = E_s \varepsilon_s \quad (5)$$

where E_s is the modulus of steel beam or steel reinforcement.

2.1.2 Assumption of steel-concrete composite beams

In order to calculate the deflection, the steel-concrete composite beam is divided into n segments from mid-span to support point, as shown in Fig. 2(a). Cross-section 1-1 is at mid-span, and cross-section 0-0 is at the end of beam. The axial force analysis of segment 1 is shown in Fig. 2(c). For simplicity, the following assumptions are used: (1) In the segment, the shear force shared by each stud shear connector is equal, and the slip of each stud shear connector is equal to the slip at the end of the segment, as shown in Eq. (6); (2) the slip at the end of each segment could be obtained by the linear integration of slip strain, as shown in Eq. (7); (3) the steel beam and the concrete deck have the same curvatures.

In fact, assumption 1 is based on the simplified distribution of stud shear connectors that the stud shear connectors all locate at the end of the segment. When the

length of the segment is small or the slip does not change significantly, the simplification is true. For assumption 2, when the length of the segment is small or the variation rate of the slip strain does not change significantly, the slip could be obtained by the linear integration of slip strain.

$$\frac{V_1}{n_1} = (1 - e^{-a\Delta_{s-2}})^b V_u \quad (6)$$

$$\Delta_{s-2} = \Delta_{s-1} + (\varepsilon_{\Delta_{s-1}} + \varepsilon_{\Delta_{s-2}}) Z_1 / 2 \quad (7)$$

where V_1 is shear force of segment 1 on the interface between concrete and steel beam; n_1 is the number of stud shear connectors in segment 1; Δ_{s-2} is the slip at cross-section 2-2; Δ_{s-1} is the slip at cross-section 1-1; $\varepsilon_{\Delta_{s-2}}$ is the slip strain at cross-section 2-2; $\varepsilon_{\Delta_{s-1}}$ is the slip strain at cross-section 1-1; Z_1 is the length of segment 1.

2.1.3 Strain distribution

The strain calculation model is shown in Fig. 2(b). From the strain-geometry relationships, the strain of each material can be written as

$$\begin{cases} \varepsilon_{as2-1} = \varepsilon_{c-1} - \phi_1 s_2 \\ \varepsilon_{as1-1} = \varepsilon_{c-1} - \phi_1 s_1 \\ \varepsilon_{c2-1} = \varepsilon_{c-1} - \phi_1 h_c \\ \varepsilon_{s2-1} = -\varepsilon_{s1-1} + \phi_1 (h - h_c - t_3 / 2) \\ \varepsilon_{\Delta_{s-1}} = \varepsilon_{s1-1} - \varepsilon_{c2-1} \\ \phi_1 = \frac{\varepsilon_{c-1} + \varepsilon_{\Delta_{s-1}}}{x_1} \end{cases} \quad (8)$$

where ε_{c-1} is the strain on the top surface of concrete in cross-section 1-1; ε_{as2-1} is the top bar strain in cross-section 1-1; ε_{as1-1} is the bottom bar strain in cross-section 1-1; ε_{c2-1} is the strain on the bottom surface of concrete in cross-section 1-1; ϕ_1 is the curvature of cross-section 1-1; ε_{s2-1} is the strain at the centerline of steel beam bottom plate in cross-section 1-1; ε_{s1-1} is the strain at the centerline of steel beam top plate in cross-section 1-1; $\varepsilon_{\Delta_{s-1}}$ is the slip strain in cross-section 1-1; x_1 is the distance from the top surface of

concrete to the neutral axis within the steel beam of cross-section 1-1; h is the distance from the top surface of concrete to the centerline of steel beam bottom plate; h_c is the depth of concrete; t_3 is the thickness of steel beam top plate; s_2 is the distance from the top surface of concrete to the centerline of top bar; s_1 is the distance from the top surface of concrete to the centerline of bottom bar.

2.1.4 Deflection calculation

According to the equilibrium conditions in segment 1, the following equations are given

$$D_{c-1} + D_{as-1} = T_{s-1} \quad (9)$$

$$M_{s-1} = \int_{x_1-h_c}^{x_1} \sigma(\varepsilon_{c-1}) b y dx + E_{as} \varepsilon_{as1-1} A_{s1} (x_1 - s_1) + E_{as} \varepsilon_{as2-1} A_{s2} (x_1 - s_2) + E_s \varepsilon_{s1-1} t_3 b_1 (x_1 - h_c - t_3 / 2) \quad (10)$$

$$D_{c-2} + D_{as-2} = T_{s-2} \quad (11)$$

$$M_{s-2} = \int_{x_2-h_c}^{x_2} \sigma(\varepsilon_{c-2}) b y dx + E_{as} \varepsilon_{as1-2} A_{s1} (x_2 - s_1) + E_{as} \varepsilon_{as2-2} A_{s2} (x_2 - s_2) + E_s \varepsilon_{s1-2} t_3 b_1 (x_2 - h_c - t_3 / 2) + \frac{1}{3} E_s \varepsilon_{s1-2} t_2 (x_2 - h_c - t_3 / 2)^2 + \frac{1}{3} E_s \varepsilon_{s2-2} t_2 (h - x_2)^2 + E_s \varepsilon_{s2-2} t_1 b_2 (h - x_2) \quad (12)$$

$$D_{c-1} + D_{as-1} - D_{c-2} - D_{as-2} = V_1 \quad (13)$$

where D_{c-1} , D_{as-1} , T_{s-1} are the resultant forces of concrete, steel bar and steel beam in cross-section 1-1, respectively; D_{c-2} , D_{as-2} , T_{s-2} are the resultant forces of concrete, steel bar and steel beam in cross-section 2-2, respectively; M_{s-1} is the bending moment in cross-section 1-1; M_{s-2} is the bending moment in cross-section 2-2; $\sigma(\varepsilon_{c-1})$ is the stress of concrete when the strain is ε_{c-1} ; A_{s2} is the area of top bar; A_{s1} is the area of bottom bar; b_1 is the width of steel beam top plate; b_2 is the width of steel beam bottom plate; t_1 is the thickness of steel beam bottom plate; t_2 is the thickness of steel beam web plate; x_2 is the distance from the top surface of concrete to the neutral axis within the steel beam of cross-section 2-2; ε_{as2-2} is the top bar strain in cross-section 2-2; ε_{as1-2} is the bottom bar strain in cross-section 2-2; ε_{s2-2} is the strain at the centerline of steel beam bottom plate in cross-section 2-2; ε_{s1-2} is the strain at the centerline of steel beam top plate in cross-section 2-2.

The resultant forces of each material in Eq. (9) can be calculated by using Eq. (14).

$$\begin{cases} D_{c-1} = \int_{x_1-h_c}^{x_1} \sigma(\varepsilon_{c-1}) b dx \\ D_{as-1} = E_{as} \varepsilon_{as1-1} A_{s1} + E_{as} \varepsilon_{as2-1} A_{s2} \\ T_{s-1} = -E_s \varepsilon_{s1-1} t_3 b_1 + E_s \varepsilon_{s2-1} t_1 b_2 + 0.5 E_s (-\varepsilon_{s1-1} + \varepsilon_{s2-1}) t_2 (h - h_c - t_3 / 2) \end{cases} \quad (14)$$

According to the calculation method of segment 1, the equilibrium equations in other segments could also be obtained. With reference to the deflection calculation method of steel-concrete composite beam¹¹, the equations could be solved by combining the boundary conditions that

$\varepsilon_{\Delta s-0} = 0$, $\Delta_{s-1} = 0$, $D_{c-0} = 0$, $D_{as-0} = 0$, $M_{u-0} = 0$. The deformation compatibility equations and the equilibrium equations in segment n can be obtained.

$$D_{c-n} + D_{as-n} = T_{s-n} \quad (15)$$

$$M_{s-n} = \int_{x_n-h_c}^{x_n} \sigma(\varepsilon_{c-n}) b y dx + E_{as} \varepsilon_{as1-n} A_{s1} (x_n - s_1) + E_{as} \varepsilon_{as2-n} A_{s2} (x_n - s_2) + E_s \varepsilon_{s1-n} t_3 b_1 (x_n - h_c - t_3 / 2) + \frac{1}{3} E_s \varepsilon_{s1-n} t_2 (x_n - h_c - t_3 / 2)^2 + \frac{1}{3} E_s \varepsilon_{s2-n} t_2 (h - x_n)^2 + E_s \varepsilon_{s2-n} t_1 b_2 (h - x_n) \quad (16)$$

$$\frac{D_{c-n} + D_{as-n} - 0}{n_n} = (1 - e^{-a\Delta_{s-0}})^b V_u \quad (17)$$

$$\Delta_{s-0} = (\varepsilon_{\Delta s-1} + \varepsilon_{\Delta s-2}) Z_1 / 2 + (\varepsilon_{\Delta s-2} + \varepsilon_{\Delta s-3}) Z_2 / 2 + \dots + (0 + \varepsilon_{\Delta s-n}) Z_n / 2 \quad (18)$$

The slip strain, slip and curvature can be obtained by solving these equations. A computer program was written to solve these equations. The larger the number of segments is, the more accurate the theoretical result is. However, the equations are not easy to solve when the number of segments is too large. After trial and error, when the composite beam is divided into 4 segments, the theoretical results could agree well with the numerical and experimental results. The flexural stiffness in each cross-section could be obtained by using Eq. (19), and the flexural stiffness at load point is used to calculate the deformation. The deflection could be obtained by using traditional structural mechanics theory.

$$B = \frac{M}{\phi} \quad (19)$$

where B is the flexural stiffness.

2.2 Deflection calculation model of GFRP-concrete-steel composite beam

The cross-section of GFRP-concrete-steel composite beam is variable. The GFRP-concrete-steel composite beam with GFRP T-rib is shown in Fig. 3(a), and the partial schematic diagram is shown in Fig. 3(b). Due to the effect of GFRP T-rib, the cross-sections in the beam direction could be divided into three types, which are the cross-sections of rib (cross-section 1-a), the cross-sections of flange (cross-section 1-b) and the cross-sections without T-rib (cross-section 1-c). For simplicity, the flange of T-rib is ignored, as shown in Fig. 3(e). In the deflection calculation model of steel-concrete composite beam, it is assumed that the slip strain distribution in each segment is linear. However, the slip strain changes significantly from the cross-section of GFRP T-rib to the cross-section without T-rib because of the effect of GFRP T-rib. Therefore, the assumption of slip strain linear distribution could not be applied directly in the calculation method of GFRP-concrete-steel composite beam. In order to consider the effect of GFRP T-rib, the GFRP-concrete-steel composite

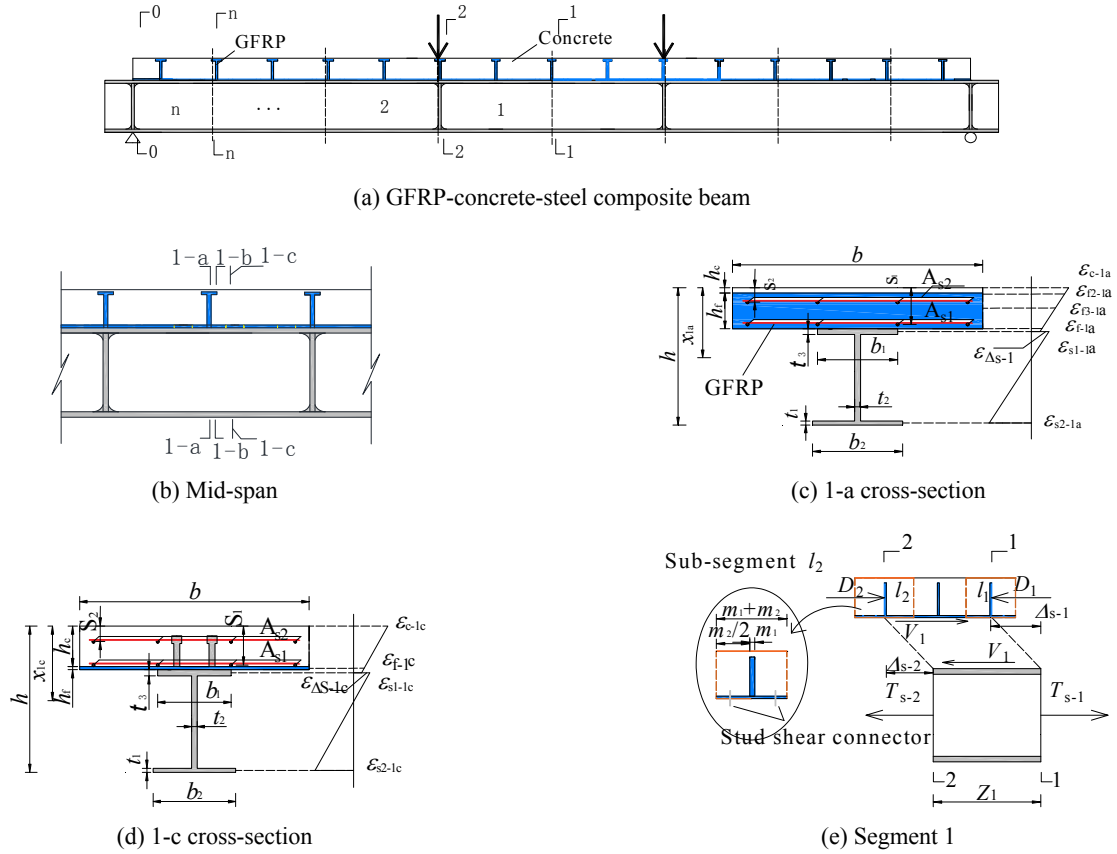


Fig. 3 Deflection calculation model of GFRP-concrete-steel composite beam

beam is divided into n segments from mid-span to support point (Fig. 3(a)), and each segment is divided into several sub-segments (Fig. 3(e)). It can be seen from Fig. 3(e) that segment 1 is divided into three sub-segments, and sub-segments l_1 and l_2 are the sub-segments at the boundary of segment 1. Each sub-segment includes one GFRP rib, and the dotted part in Fig. 3(e) is the GFRP-concrete deck in the sub-segment. In order to calculate the deflection of GFRP-concrete-steel composite beam, the following assumptions are used:

- (1) The bending moment does not change in the sub-segment and is equal to the bending moment in the middle of the sub-segment;
- (2) The shear connectors all locate at the end of the sub-segment, and do not play a role in the sub-segment;
- (3) The equivalent slip strain distribution is linear in the segment, the calculation equation of the equivalent slip strain of sub-segment l_1 is shown in Eq. (20), and the slip at the end of segment 1 can be obtained by using Eq. (21);
- (4) In the segment, the shear force shared by each stud shear connector is equal, and the slip of each stud shear connector is equal to the slip at the end of the segment;
- (5) The steel beam and the GFRP-concrete deck have the same curvature;
- (6) The slip between GFRP plate and concrete is ignored.

$$\frac{\varepsilon_{\Delta s-1a} m_1 + \varepsilon_{\Delta s-1c} m_2}{m_1 + m_2} = \varepsilon_{\Delta s-1eq} \quad (20)$$

$$\Delta_{s-2} = \Delta_{s-1} + (\varepsilon_{\Delta s-1eq} + \varepsilon_{\Delta s-2eq}) Z_1 / 2 \quad (21)$$

where $\varepsilon_{\Delta s-1a}$ is the slip strain in cross-section 1-a; $\varepsilon_{\Delta s-1c}$ is the slip strain in cross-section 1-c; m_1 is the thickness of GFRP rib; m_2 is the length of the sub-segment without GFRP rib; $\varepsilon_{\Delta s-1eq}$ is the equivalent slip strain of sub-segment l_1 ; $\varepsilon_{\Delta s-2eq}$ is the equivalent slip strain of sub-segment l_2 .

According to assumption 1, the equilibrium equations in sub-segment l_1 can be obtained, as shown in Eqs. (22) to (25). The equilibrium equations in sub-segment l_2 can be obtained by using the same method and are not listed.

$$D_{c-1a} + D_{as-1a} + D_{f-1a} = T_{s-1a} \quad (22)$$

$$\begin{aligned} M_{s-1} = & \int_{x_{1a}-h_c}^{x_{1a}} \sigma(\varepsilon_{c-1a}) b y dx + E_{as} \varepsilon_{as-1a} A_{s1} (x_{1a} - s_1) \\ & + E_{as} \varepsilon_{as-2-1a} A_{s2} (x_{1a} - s_2) + \int_{x_{1a}-h_c}^{x_{1a}-h_f} \sigma(\varepsilon_{f3-1a}) b y dx \\ & + E_s \varepsilon_{s1-1a} t_3 b_1 (x_{1a} - h_c - h_f - t_3 / 2) \\ & + \frac{1}{3} E_s \varepsilon_{s1-1a} t_2 (x_{1a} - h_c - h_f - t_3 / 2)^2 \\ & + \frac{1}{3} E_s \varepsilon_{s2-1a} t_2 (h - x_{1a})^2 + E_s \varepsilon_{s2-1a} t_1 b_2 (h - x_{1a}) \end{aligned} \quad (23)$$

$$D_{c-1c} + D_{as-1c} + D_{f-1c} = T_{s-1c} \quad (24)$$

$$\begin{aligned}
M_{s-1} = & \int_{x_{1c}-h_c}^{x_{1c}} \sigma(\varepsilon_{c-1c}) b y dx + E_{as} \varepsilon_{as1-1c} A_{s1} (x_{1c} - s_1) \\
& + E_{as} \varepsilon_{as2-1c} A_{s2} (x_{1c} - s_2) + E_f \varepsilon_{f-1c} b h_f (x_{1c} - h_c - h_f / 2) \\
& + E_s \varepsilon_{s1-1c} t_3 b_1 (x_{1c} - h_c - h_f - t_3 / 2) \\
& + \frac{1}{3} E_s \varepsilon_{s1-1c} t_2 (x_{1c} - h_c - h_f - t_3 / 2)^2 \\
& + \frac{1}{3} E_s \varepsilon_{s2-1c} t_2 (h - x_{1c})^2 + E_s \varepsilon_{s2-1c} t_1 b_2 (h - x_{1c})
\end{aligned} \quad (25)$$

where D_{c-1a} , D_{as-1a} , D_{f-1a} , T_{s-1a} are the resultant forces of concrete, steel bar, GFRP plate, steel beam in cross-section 1-a, respectively; D_{c-1c} , D_{as-1c} , D_{f-1c} , T_{s-1c} are the resultant forces of concrete, steel bar, GFRP plate, steel beam in cross-section 1-c, respectively; M_{s-1} is the bending moment in sub-segment l_1 ; x_{1a} , x_{1c} are the distances of cross-section 1-a and cross section 1-c from the top surface of concrete to the neutral axis within the steel beam, respectively; ε_{as1-1a} , ε_{as2-1a} , ε_{c-1a} are the strains of bottom bar, top bar and the top surface of concrete in cross-section 1-a, respectively; ε_{f3-1a} is the strain of GFRP rib in cross-section 1-a; $\sigma(\varepsilon_{f3-1a})$ is the stress of GFRP rib when the strain is ε_{f3-1a} ; ε_{s1-1a} , ε_{s2-1a} are the strains at the centerline of steel beam top plate and steel beam bottom plate in cross-section 1-a; ε_{as1-1c} , ε_{as2-1c} , ε_{c-1c} are the strains of bottom bar, top bar and the top surface of concrete in cross-section 1-c; ε_{f-1c} is the strain at the centerline of GFRP bottom plate in cross-section 1-c; ε_{s1-1c} , ε_{s2-1c} are the strains at the centerline of steel beam top plate and steel beam bottom plate in cross-section 1-c.

The axial force equilibrium equation in segment 1 is as followed

$$D_1 - D_2 = V_1 \quad (26)$$

where D_1 is the resultant force of GFRP-concrete deck in sub-segment l_1 ; D_2 is the resultant force of GFRP-concrete deck in sub-segment l_2 .

According to assumption 2, the stud shear connector locates at the end of the sub-segment, and there is no stud shear connector in the sub-segment. The axial force equilibrium equations in the sub-segment are as followed

$$D_{c-1a} + D_{as-1a} + D_{f-1a} = D_{c-1c} + D_{as-1c} + D_{f-1c} = D_1 \quad (27)$$

$$D_{c-2a} + D_{as-2a} + D_{f-2a} = D_{c-2c} + D_{as-2c} + D_{f-2c} = D_2 \quad (28)$$

Substituting Eqs. (21) and (26) into Eq. (6) obtains

$$\frac{D_1 - D_2}{n_1} = (1 - e^{-a(\Lambda_{s-1} + (\varepsilon_{as-1c} + \varepsilon_{as-2c}) Z_1 / 2)})^b V_u \quad (29)$$

where D_{c-2a} , D_{as-2a} , D_{f-2a} , T_{s-2a} are the resultant forces of concrete, steel bar, GFRP plate, steel beam in cross-section 2-a, respectively; D_{c-2c} , D_{as-2c} , D_{f-2c} , T_{s-2c} are the resultant forces of concrete, steel bar, GFRP plate, steel beam in cross-section 2-c, respectively.

Similarly, the equations in other segments of GFRP-concrete-steel composite beam can be obtained. The force, strain and boundary condition can be obtained by referring to the calculation method of steel-concrete composite beam.

Then the slip strain, slip and curvature can be obtained by solving these equations. The equivalent flexural stiffness at load point is used to calculate the deflection. The equivalent flexural stiffness of sub-segment l_2 can be obtained by using Eq. (30), and the deflection could be obtained by using traditional structural mechanics theory.

$$\phi_{2eq} = \frac{\phi_{2-a} m_1 + \phi_{2-c} m_2}{m_1 + m_2} \quad (30)$$

where ϕ_{2-a} is the curvature in cross-section 2-a; ϕ_{2-c} is the curvature in cross-section 2-c; ϕ_{2eq} is the equivalent curvature of sub-segment l_2 .

3. Experimental verification

In order to verify the accuracy of proposed theoretical model, three composite beams (specimens S-1 to S-3) were fabricated and tested. Specimens S-1 and S-3 were GFRP-concrete-steel composite beams, and specimen S-2 was steel-concrete composite beam. The sizes of three composite beams were the same. The calculation span was 3000 mm, the diameter of the stud shear connector was 13 mm, and the spacing of the stud shear connector was 100 mm. The stud shear connectors were embedded in the concrete through the holes of GFRP bottom plate, as shown in Fig. 4(e). The wet adhesive bond interface between GFRP bottom plate and concrete was used in specimen S-1, as shown in Fig. 4(f). The unbonded interface was used in specimen S-3. The cross-sections of specimens S-1 and S-3 were shown in Fig. 4(a), the loading test system was shown in Fig. 4(d), and the cross-section of specimen S-2 was shown in Fig. 4(b).

The cubic concrete strengths of specimens S-1 to S-3 were 36.2 MPa, 40.6 MPa and 39.1 MPa, respectively. The yield strengths of 8 mm and 12 mm Q345 steel plate were 502 MPa and 428 MPa, and the ultimate strengths were 568 MPa and 554 MPa. The yield and ultimate strengths of 6 mm HRB 400 steel bar were 440 MPa and 610 MPa. The tensile strength and compressive strength of GFRP plate in the transverse direction were 80.9 MPa and 103.5 MPa, and the modulus was 1.08×10^4 MPa. The tensile strength of stud shear connector was 460 MPa. The shear capacity and the load-slip curve of the shear connector of GFRP-concrete-steel composite were similar to that of steel-concrete composite beam, the load-slip curve could be obtained by using Eq. (31), and the shear capacity of stud shear connector could be calculated by using Eq. (3). (Gao 2017)

$$V / V_u = (1 - e^{-1.13s})^{0.49} \quad (31)$$

The FE model was also checked by experiments. The ANSYS program was used to model the experimental beams. An eight node 3-D concrete element (SOLID65) was used to model the concrete, and the uniaxial stress-strain relationship was obtained by using Eq. (1). An eight node 3-D orthotropic element (SOLID185) was used to model the GFRP plate, the steel bar was simulated by 3D spar element LINK8, and the steel beam was simulated by

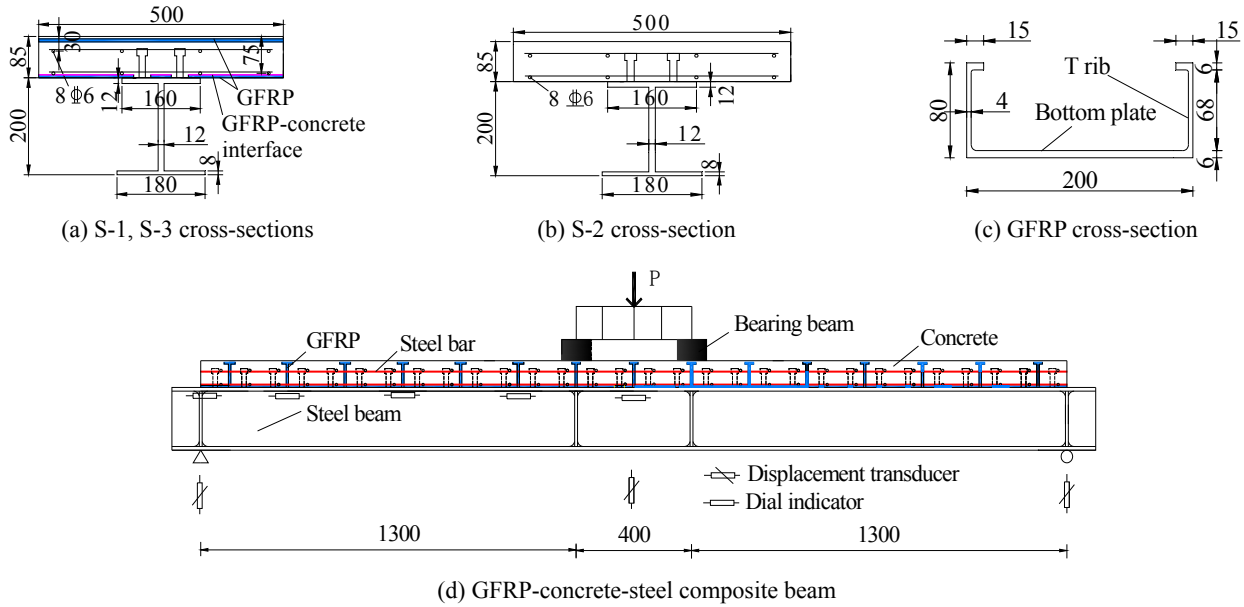


Fig. 4 Overview of composite beam layout and fabrication (mm)

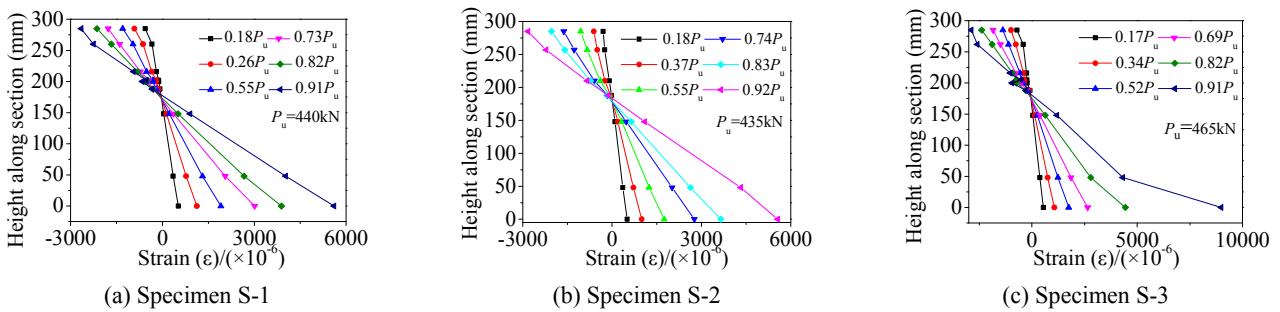


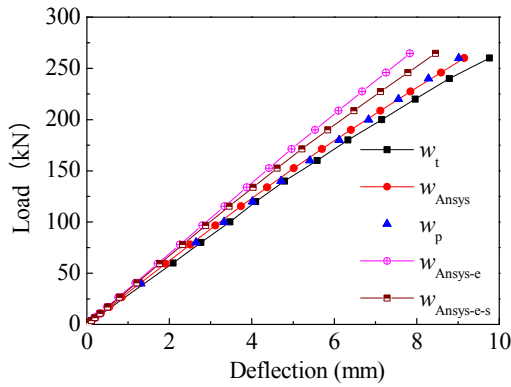
Fig. 5 Strain distribution

shell element SHELL181. The elastic constitutive relationship was used for GFRP plate, steel bar and steel beam. The steel bar and the GFRP-concrete deck were connected by common nodes, and the GFRP plate and the concrete were also connected by common nodes. The spring element (COMBINE39) was used to simulate the stud shear connector in the beam direction, and the load-slip relationship expressed in Eq. (31) was used. In other directions, the GFRP-concrete deck and the steel beam were connected by coupled nodes.

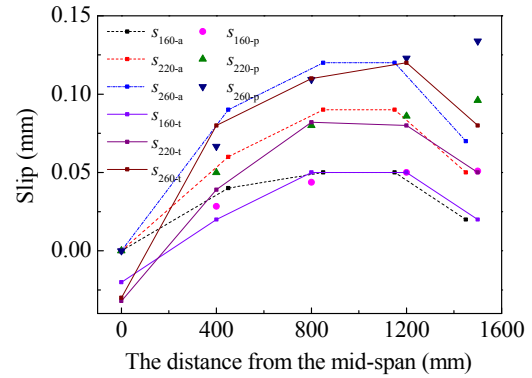
Fig. 5 shows the strain distribution at mid-span. The strain of top surface of concrete, steel bar, GFRP bottom plate, and steel beam were measured. It can be seen that the plane cross section of specimens S-1 and S-3 remained plane before $0.73P_u$. The slip occurred at the interface

between GFRP-concrete deck and steel beam at about $0.73P_u$, and a higher load resulted in a larger slip. Before the ultimate load, the strains of the GFRP bottom plate, top bar and bottom bar of specimens S-1 and S-3 were in a straight line. This phenomenon shows the slip between GFRP plate and concrete could be ignored. For specimen S-3 with unbonded interface, although the surface between GFRP bottom plate and concrete was smooth, the GFRP plate was restrained by the GFRP ribs and the stud shear connectors. Therefore, there was no obvious slip between GFRP plate and concrete.

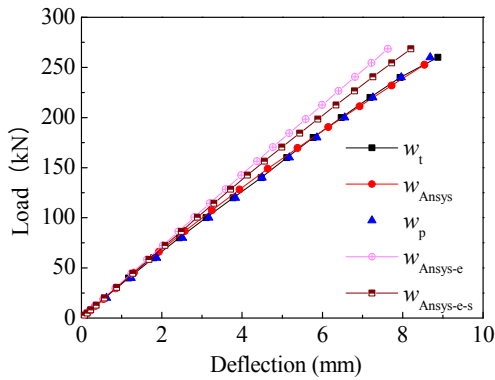
Fig. 6 shows the comparison of theoretical, numerical and experimental results. The comparisons of deflection were shown in Figs. 6(a), (c) and (e). w_t represents the experimental deflection, w_{Anslys} represents the numerical



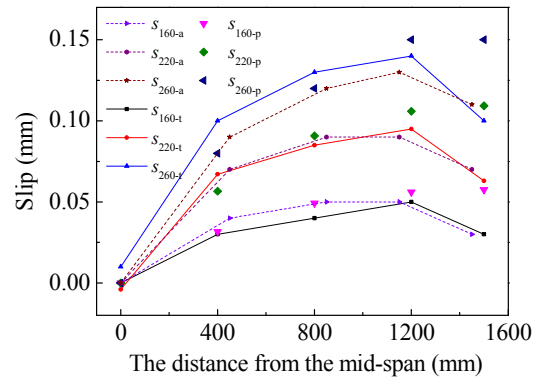
(a) Load-deflection curves of specimen S-1



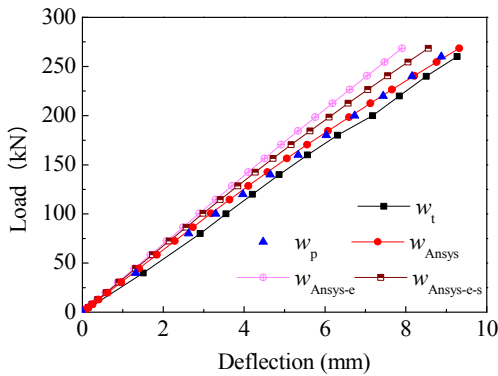
(b) The slip of specimen S-1



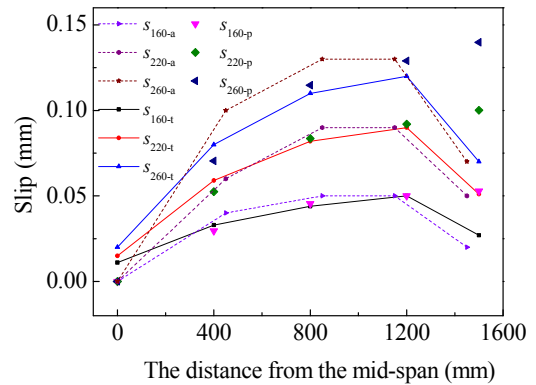
(c) Load-deflection curves of specimen S-2



(d) The slip of specimen S-2



(e) Load-deflection curves of specimen S-3



(f) The slip of specimen S-3

Fig. 6 Comparison of theoretical, numerical and experimental results

deflection results which consider concrete nonlinearity and slip, $w_{\text{Ansys-e}}$ represents the numerical deflection results which ignore slip and concrete nonlinearity, $w_{\text{Ansys-e-s}}$ represents the numerical deflection results which ignore concrete nonlinearity and consider slip, w_p represents the theoretical results. $w_{\text{Ansys-e}}$, $w_{\text{Ansys-e-s}}$, w_{Ansys} represent the results by using transformed section method, the calculation method considering slip, and the calculation method considering slip and concrete nonlinearity, respectively. It can be seen from Figs. 6(a), (c) and (e) that the concrete nonlinearity and the slip had an obvious effect on the deflection calculation results of experimental beams. The theoretical results (w_p) agreed well with the numerical results (w_{Ansys}). However, the experimental results were slightly lower than the numerical and theoretical results.

The reason may be that there was deviation in the fabrication of composite beams. In general, the deflection of composite beams could be predicted by using the theoretical and numerical calculation method.

Figs. 6(b), (d) and (f) show the comparison of slip. S_{160-a} , S_{160-t} , S_{160-p} represent the numerical results, the experimental results and the theoretical results at 160 kN, S_{220-a} , S_{220-t} , S_{220-p} represent the numerical results, the experimental results and the theoretical results at 220 kN, S_{260-a} , S_{260-t} , S_{260-p} represent the numerical results, the experimental results and the theoretical results at 260 kN. It can be seen from Figs. 6(b), (d) and (f) that the numerical results agreed well with the experimental results. The slip increased from the mid-span to the end of the beam and decreased slightly near the end of the beam. In the range of 800 mm from the

Table 1 Details of finite element models

Specimen	Number of stud shear connector n	Studs spacing	Number of studs in each row	Type of GFRP plate	$m_1/(m_1+m_2)$	Height of rib (mm)
A-1	60	100	2	—	—	—
A-2	30	100	1	—	—	—
A-3	15	200	1	—	—	—
G-1	60	100	2	I	0.24	80
G-2	30	100	1	I	0.24	80
G-3	15	200	1	I	0.24	80
H-1	30	100	1	II	0.24	55
H-2	15	200	1	II	0.24	55

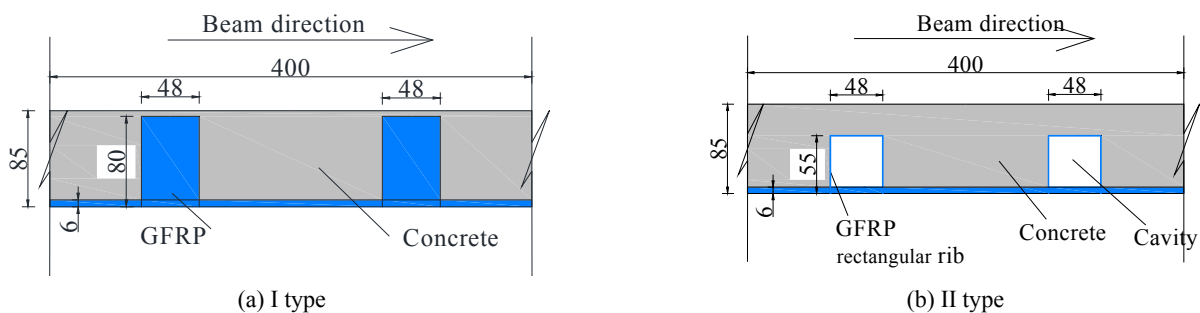


Fig. 7 GFRP-concrete decks

mid-span, the theoretical results agreed well with the numerical and experimental results. However, there was a large deviation between the theoretical results and the experimental and numerical results near the end of the beam. The theoretical slip increased from the mid-span to the end of the beam, and the maximum slip was at the end of the beam. The theoretical slip distribution was the same as that in the literature (Nie and Cai 2003). The deviation of the slip distribution may be due to the boundary condition assumption. However, the deviation of the slip near the end of the beam was caused by the slip strain near the end of the beam, and the coincidence between the predicted slip and the experimental and numerical slip near the mid-span showed that the deviation of the theoretical model had small effect on the slip strain near the mid-span. Therefore, the deflection of the composite beams could be predicted by using the theoretical method.

4. Comparison of theoretical and numerical results

In order to further verify the accuracy of the deformation calculation method, the theoretical model was checked with more nonlinear finite element models, which included different GFRP plates and numbers of stud shear connectors. Table 1 shows the parameters of the finite element models. $m_1 / (m_1 + m_2)$ represents the proportion of GFRP plate in the GFRP-concrete deck, m_1 represents the thickness of GFRP rib, m_2 represents the length of the subsegment without GFRP rib. The size, material and load position of the composite beams in Table 1 were the same as that of specimen S-1. The stud shear connectors were

arranged with equal intervals. Specimens A-1, A-2 and A-3 were steel-concrete composite beams with different numbers of studs, and they were used to verify the accuracy of the steel-concrete composite beam calculation method. Specimens G-1, G-2, and G-3 were GFRP-concrete-steel composite beams with I type GFRP plate, and the thickness of GFRP rib was enlarged to increase the effect of GFRP rib on the deflection. Specimens H-1, H-2 were GFRP-concrete-steel composite beams with II type GFRP plate, and the cavity was caused by the rectangular rib. The GFRP rectangular rib was ignored in the deflection calculation, and only the cavity was considered. The details of I type GFRP plate and II type GFRP plate are shown in Fig. 7.

Fig. 8(a) shows the comparison of theoretical and numerical results of steel-concrete composite beams. w_{A-1-p} , w_{A-2-p} , w_{A-3-p} represent the theoretical results of specimens A-1, A-2 and A-3, w_{A-1-a} , w_{A-2-a} , w_{A-3-a} represent the numerical result of specimens A-1, A-2 and A-3. It can be seen from Fig. 8(a) that a lower number of stud shear connectors resulted in a larger deflection, and the growth rate of the deflection increased with the decrease of the number of studs. The load-deflection curves of specimens A-1, A-2 and A-3 were significantly different because of slip. The theoretical results agreed well with the numerical results, and the deflection of steel-concrete composite beams with full or partial shear connectors can be predicted by using the theoretical method.

Fig. 8(b) shows the comparison of theoretical and numerical results of GFRP-concrete-steel composite beams with I type GFRP plate, and Fig. 8(c) shows the comparison of theoretical and numerical results of GFRP-concrete-steel composite beams with II type GFRP plate. w_{G-1-p} , w_{G-2-p} ,

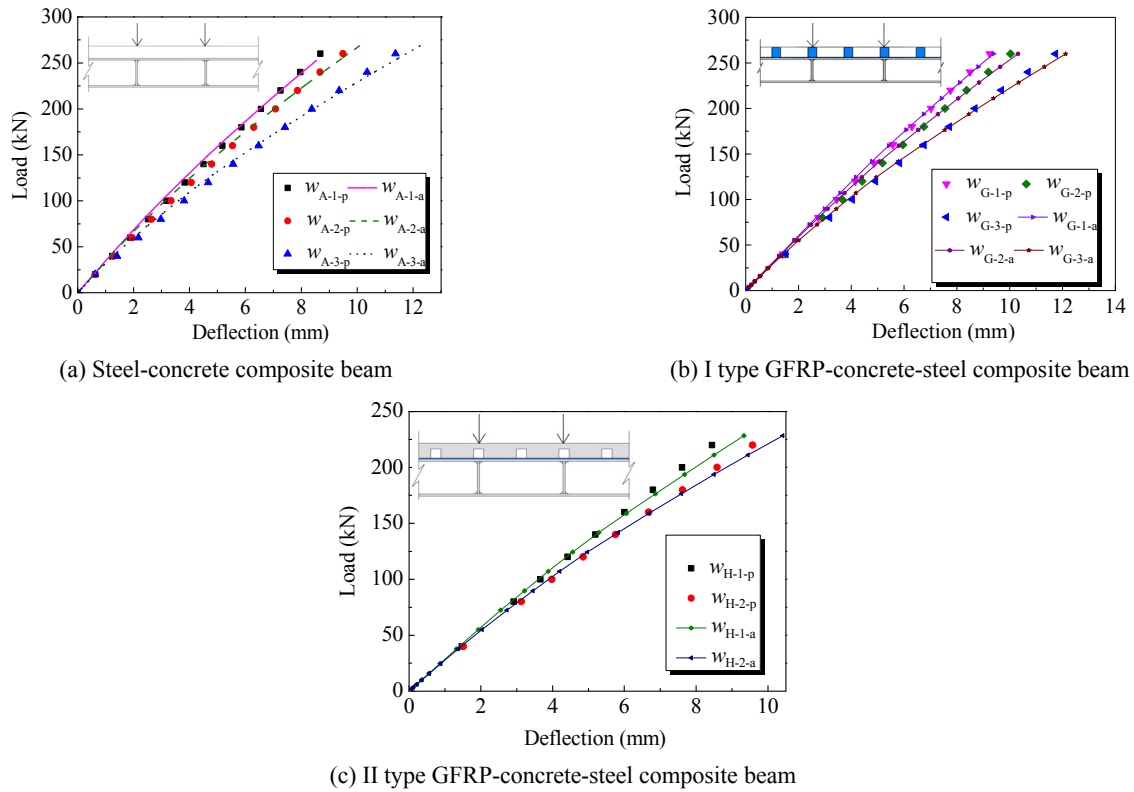


Fig. 8 Comparison of numeral and theoretical results

w_{G-3-p} , w_{H-1-p} , w_{H-2-p} represent the theoretical results of specimens G-1, G-2, G-3, H-1, H-2, and w_{G-1-a} , w_{G-2-a} , w_{G-3-a} , w_{H-1-a} , w_{H-2-a} represent the numeral results of specimens G-1, G-2, G-3, H-1, H-2. It can be seen from Figs. 8(b) and 8(c) that the theoretical results agreed well with the numeral results and the deflection of GFRP-concrete-steel composite beam could be predicted by using the theoretical method.

5. Parametric analysis

The accuracy of the theoretical method had been verified in the previous sections. The effect of GFRP rib on the deflection was discussed in this section. Specimens S-1 was used to perform the parametric analysis.

Fig. 9 shows the relationship of specimen S-1 between the thickness of GFRP rib and the equivalent curvature at 200 kN. The relationship at other load is similar. Φ represents the equivalent curvature with different rib thickness at the load point, Φ_0 represents the equivalent curvature at the load point when $m_1/(m_1+m_2)$ is zero, n represents the number of stud shear connector. It can be seen from Fig. 9 the relationship between the rib thickness and the equivalent curvature was linear. With the increase of the GFRP rib thickness, the equivalent curvature of composite beams increased because of the low modulus of GFRP. From the comparison of GFRP-concrete-steel composite beams with different numbers of studs, it can be seen that the effect of GFRP rib thickness on the equivalent curvature decreased with the reduction of the number of studs. The reason was that the slip of composite beams

increased with the decrease of the number of studs, and the bending moment shared by GFRP-concrete decks decreased. Therefore, the effect of GFRP-concrete deck on the flexural stiffness was reduced, and the effect of GFRP rib thickness on the equivalent curvature decreased.

Fig. 10 shows the relationship of specimen S-1 between the height of GFRP rib and the equivalent curvature at 200 kN when $m_1 / (m_1 + m_2)$ is 0.24. Φ represents the equivalent curvature with different rib heights at the load point, Φ_0 represents the equivalent curvature at the load point when there was no GFRP rib. It can be seen from Fig. 10 that a higher height of GFRP rib resulted in a larger equivalent curvature. Moreover, the effect of GFRP rib height on the equivalent curvature decreased with the reduction of the number of studs. The reason was the same as that of GFRP rib thickness.

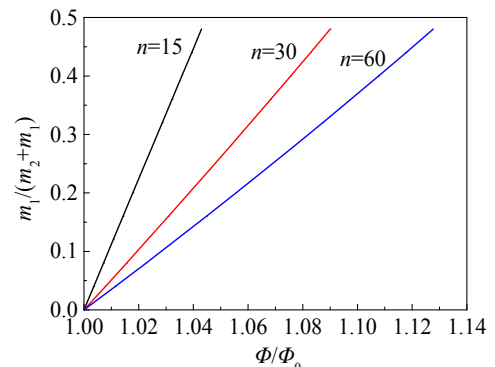


Fig. 9 The relationship between the thickness of GFRP rib and the equivalent curvature

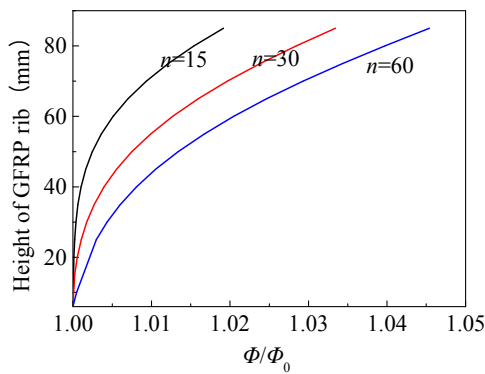


Fig. 10 The relationship between the height of GFRP rib and the equivalent curvature

From the relationship between GFRP rib and equivalent curvature, it can be seen the effect of GFRP rib on the deflection increased with the increase of the number of studs. The relationship is shown in Eq. (32).

$$\frac{\phi_b}{\phi_{b-0}} < \frac{\phi_a}{\phi_{a-0}} \quad (32)$$

where ϕ_a is the equivalent curvature of GFRP-concrete-steel composite beams without consideration of slip; ϕ_{a-0} is the equivalent curvature of GFRP-concrete-steel composite beams without consideration of slip and GFRP rib; ϕ_b is the equivalent curvature of GFRP-concrete-steel composite beams considering slip; ϕ_{b-0} is the equivalent curvature of GFRP-concrete-steel composite beams, which considers slip and ignores GFRP rib.

According to the Eq. (32), the equation can be obtained

$$\phi_b < k\phi_{b-0} \quad (33)$$

where k is the ratio coefficient, $k = \phi_a / \phi_{a-0}$.

According to the curvature-deflection relationship, the equation can be obtained

$$w_b < kw_{b-0} \quad (34)$$

where w_b is the deflection of GFRP-concrete-steel composite beams; w_{b-0} is the deflection of GFRP-concrete-steel composite beams without consideration of GFRP rib.

It can be seen from Eq. (34) that the deflection of GFRP-concrete-steel composite beam can be roughly predicted by using the ratio coefficient k of GFRP-concrete-steel composite beam without consideration of slip. The ratio coefficient k can be obtained by using the sectional analysis method without consideration of slip. The deflection w_{b-0} of GFRP-concrete-steel composite beam without consideration of GFRP rib can be obtained by using the method of steel-concrete composite beams in the previous section. Then the deflection w_b of GFRP-concrete-steel composite beam can be estimated by the product of k and w_{b-0} .

As Eq. (34) is calculated by using the theoretical method of steel-concrete composite beam and the equilibrium equation of sub-segments need not to be established, the

number of equations is greatly reduced. Therefore, the equations are easy to solve by using the simplified calculation formula. Moreover, in the design of GFRP-concrete-steel composite beam, the predicted result by using Eq. (34) is conservative.

6. Conclusions

This paper investigated the deflection calculation method of GFRP-concrete-steel composite beam. The following conclusions can be drawn:

- The deflection calculation method of composite beam was exhibited, which considered slip, concrete nonlinearity, and variable cross-sections. The accuracy of the theoretical model was verified by experiment and FE models. Although the composite beams with GFRP T-rib and the composite beams with GFRP rectangular rib are used to verify the accuracy of the theoretical method, it can be seen that the deflection of composite beams with other types of GFRP plate can be predicted by using the calculation method. In general, the deflection of steel-concrete/GFRP-concrete-steel composite beams with full or partial shear connectors could be predicted by using the theoretical method before the bending moment achieved the elastic bending moment capacity.
- The deflection and slip of GFRP-concrete-steel composite beams could be predicted by using the nonlinear finite element simulation method in the paper. The comparison of the FE models established with different methods showed concrete nonlinearity and slip had an obvious effect on the deflection.
- From the parametric analysis, it can be seen that the equivalent curvature increased with the increase of rib thickness and rib height, and the effect on the equivalent curvature decreased with the reduction of the number of studs. Based on the parametric analysis, a simplified deflection calculation formula of GFRP-concrete-steel composite beam was exhibited. This calculation formula reduced the number of equations and was easier to solve.

Acknowledgments

The author(s) declared no potential conflicts of interest with respect to the research, authorship, and publication of this article. The author(s) disclosed receipt of the following financial support for the research, authorship, and publication of this article: This article was supported by the financial support provided by China Communications Construction Company Ltd. under grant No. 271400140114.

References

- Alagusundaramoorthy, P., Harik, I.E. and Choo, C.C. (2006), "Structural behavior of FRP composite bridge deck panels", *J. Bridge Eng.*, **11**(4), 384-393.

- Aref, A.J., Chiewanichakorn, M., Chen, S.S. and Ahn, I.S. (2007), "Effective slab width definition for negative moment regions of composite bridges", *J. Bridge Eng.*, **12**(3), 339-349.
- Berg, A.C., Bank, L.C., Oliva, M.G. and Russell, J.S. (2006), "Construction and cost analysis of an FRP reinforced concrete bridge deck", *Constr. Build. Mater.*, **20**(8), 515-526.
- Cheng, L. (2011), "Flexural fatigue analysis of a CFRP form reinforced concrete bridge deck", *Compos. Struct.*, **93**(11), 2895-2902.
- Cho, K., Park, S.Y., Kim, S.T., Cho, J.R. and Kim, B.S. (2013), "Behavioral characteristics of precast FRP-concrete composite deck subjected to combined axial and flexural loads", *Compos. B*, **44**(1), 679-685.
- Dieter, D.A., Dietsche, J.S., Bank, L.C., Oliva, M. and Russell, J. (2002), "Concrete bridge decks constructed with fiber-reinforced polymer stay-in-place forms and grid reinforcing", *Transp. Res. Rec.: J. Transp. Res. Board*, **1814**, 219-226.
- Gao, D. (2017), "Experimental research on GFRP-concrete-steel composite bridge decks and shear connections", Master Dissertation; Southeast University, Nanjing, China.
- Goncalves, R. and Camotim, D. (2010), "Steel-concrete composite bridge analysis using generalised beam theory", *Steel Compos. Struct., Int. J.*, **10**(3), 223-243.
- Hanswille, G., Porsch, M. and Ustundag, C. (2007a), "Resistance of headed studs subjected to fatigue loading: Part I: Experimental study", *J. Constr. Steel Res.*, **63**(4), 475-484.
- Hanswille, G., Porsch, M. and Ustundag, C. (2007b), "Resistance of headed studs subjected to fatigue loading Part II: Analytical study", *J. Constr. Steel Res.*, **63**(4), 485-493.
- He, J., Liu, Y.Q., Chen, A.R. and Dai, L. (2012), "Experimental investigation of movable hybrid GFRP and concrete bridge deck", *Constr. Build. Mater.*, **26**(1), 49-64.
- Honickman, H., Nelson, M. and Fam, A. (2009), "Investigation into the bond of glass fiber-reinforced polymer stay-in-place structural forms to concrete for decking applications", *Transp. Res. Rec.: J. Transp. Res. Board*, **2131**, 134-144.
- Huang, Y., Huang, D., Yang, Y., Yi, W.J. and Zhu, Z.G. (2016), "Element-based effective width for deflection calculation of steel-concrete composite beams", *J. Constr. Steel Res.*, **121**, 163-172.
- JTGT D64-01-2015 (2015), Specifications for design and construction of highway steel-concrete composite bridge, MOT; Beijing, China.
- Khorramian, K., Maleki, S., Shariati, M., Jalali, A., and Tahir, M. M. (2017), "Numerical analysis of tilted angle shear connectors in steel-concrete composite systems", *Steel Compos. Struct., Int. J.*, **23**(1), 67-85.
- Moses, J.P., Harries, K.A., Earls, C.J. and Yulimana, W. (2006), "Evaluation of effective width and distribution factors for GFRP bridge decks supported on steel girders", *J. Bridge Eng.*, **11**(4), 401-409.
- Nelson, M. and Fam, A. (2012), "Structural GFRP permanent forms with T-shape ribs for bridge decks supported by precast concrete girders", *J. Bridge Eng.*, **18**(9), 813-826.
- Nelson, M. and Fam, A. (2014), "Modeling of flexural behavior and punching shear of concrete bridge decks with FRP stay-in-place forms using the theory of plates", *J. Eng. Mech.*, **140**(12), 04014095.
- Nie, J.G. and Cai, C.S. (2003), "Steel-concrete composite beams considering shear slip effects", *J. Struct. Eng.*, **129**(4), 495-506.
- Nie, J., Cai, C.S. and Wang, T. (2005), "Stiffness and capacity of steel-concrete composite beams with profiled sheeting", *Eng. Struct.*, **27**(7), 1074-1085.
- Ranzi, G. and Zona, A. (2007), "A steel-concrete composite beam model with partial interaction including the shear deformability of the steel component", *Eng. Struct.*, **29**(11), 3026-3041.
- Samaaneh, M.A., Sharif, A.M., Baluch, M.H. and Azad, A.K. (2016), "Numerical investigation of continuous composite girders strengthened with CFRP", *Steel Compos. Struct., Int. J.*, **21**(6), 1307-1325.
- Tanchev, R.T. (1996), "Shear lag in orthotropic beam flanges and plates with stiffeners", *Int. J. Solids Struct.*, **33**(9), 1317-1334.
- Wang, Y.C. (1998), "Deflection of steel-concrete composite beams with partial shear interaction", *J. Struct. Eng.*, **124**(10), 1159-1165.
- Wang, W.W., Dai, J.G. and Harries, K.A. (2013), "Intermediate crack-induced debonding in RC beams externally strengthened with prestressed FRP laminates", *J. Reinf. Plast. Comp.*, **32**(23), 1842-1857.
- Zheng, Y.Z., Wang, W.W. and Brigham, J.C. (2016), "Flexural behavior of reinforced concrete beams strengthened with a composite reinforcement layer: BFRP grid and ECC", *Constr. Build. Mater.*, **115**, 424-437.
- Zhou, W.B., Li, S.J., Jiang, L.Z. and Qin, S.Q. (2015), "Vibration analysis of steel-concrete composite box beams considering shear lag and slip", *Math. Probl. Eng.*, **2015**(1), 1-8.
- Zou, B., Chen, A., Davalos, J.F. and Salim, H.A. (2011), "Evaluation of effective flange width by shear lag model for orthotropic FRP bridge decks", *Compos. Struct.*, **93**(2), 474-482.

DL